Universidad
Industrial de
Santander

UIS

Aerodynamic analysis of unmanned aerial vehicle with hawk shape for monitoring oil leakage

Análisis aerodinámico de un vehículo aéreo no tripulado con forma de halcón para monitoreo de fugas de hidrocarburos

**Christopher Fuentes-Hernández [1a], Ernesto A. Elvira-Hernández [2],
Oliver M. Huerta-Chávez [3], Héctor Vázquez-Leal [4], Marco O. Vigueras-Zúñiga [1b],
Agustín L. Herrera-May [1c]**

[1] Maestría en Ingeniería Aplicada, Facultad de Ingeniería de la Construcción y el Hábitat, Universidad Veracruzana, México. Emails: [a] fuentes_1290@hotmail.com, [b] mvigueras@uv.mx, [c] leherrera@uv.mx.
Orcid: [b] 0000-0002-2466-1458, [c] 0000-0002-7373-9258
[2] Micro and Nanotechnology Research Center, Universidad Veracruzana, México.
Email: aelvirah@hotmail.com. Orcid: 0000-0003-1407-3051.
[3] Tecnológico de Estudios Superiores de Ecatepec, Tecnológico Nacional de México, México.
Email: lecram_21@hotmail.com. Orcid: 0000-0002-2932-2033.
[4] Facultad de Instrumentación Electrónica, Universidad Veracruzana, México. Email: hvazquez@uv.mx.
Orcid: 0000-0002-7785-5272.

Abstract

The oil pipeline network requires periodic monitoring to detect pipeline damages, which may cause oil leakage with severe environmental contamination. These damages can be generated by interference from third parties such as construction works, sabotage, vandalism, excavations, and illegal oil theft. To detect the oil pipeline damages, it can be used aerodynamic aerial vehicles (UAVs) with infrared cameras and image processing systems. This paper presents the aerodynamic analysis of a UAV with a hawk shape (wingspan of 2.20 m and length of 1.49 m) for potential application in the detection of oil pipeline failures. A 1:6.5 scale prototype of the UAV is fabricated using a 3D printer. The aerodynamic coefficients of UAV are determined using computational fluid dynamic (CFD) simulations and experimental testing with a subsonic wind tunnel. In addition, the lift and drag coefficients of UAVs are obtained as a function of Reynolds number and angle of attack. Also, the air velocity profile around UAV is estimated with the CFD model. The proposed UAV could decrease the inspection costs of pipeline networks in comparison with the use of helicopters or light aircraft.

Keywords: aerodynamic analysis; infrared camera; computational fluid dynamics; drag coefficient; lift coefficient; oil leakage; oil industry; oil pipeline; subsonic wind tunnel; unmanned aerial vehicle.

Resumen

La red de oleoductos requiere monitoreo periódico para detectar daños que puedan causar fugas de hidrocarburos con severo daño ambiental. Estos daños pueden generarse por interferencia de terceros, tales como trabajos de construcción, sabotaje, vandalismo, excavaciones y sustracción ilegal de hidrocarburos. Para detectar daños en

oleoductos pueden utilizarse vehículos aéreos no tripulados (UAVs) con cámaras infrarrojas y sistemas de procesamiento de imágenes. Este trabajo presenta el análisis aerodinámico de un UAV con forma de halcón (envergadura de 2,20 m y longitud de 1,49 m) para aplicación potencial en la detección de fallas de oleoductos. Un prototipo a escala de 1:6,5 es fabricado usando una impresora 3D. Los coeficientes aerodinámicos del UAV son determinados usando simulaciones de dinámica de fluidos computacionales (CFD) y pruebas experimentales con un túnel de viento subsónico. Además, los coeficientes de sustentación y arrastre del UAV son obtenidos como función del número de Reynolds y el ángulo de ataque. También, el perfil de velocidad del aire alrededor del UAV es estimado con el modelo CFD. El UAV propuesto podría disminuir los costos de inspección de oleoductos en comparación con el uso de helicópteros o vehículos aéreos ligeros.

Palabras clave: análisis aerodinámico; cámara infrarroja; dinámica de fluidos computacionales; coeficiente de arrastre; coeficiente de sustentación; fuga de hidrocarburos; industria petrolera; oleoductos; túnel de viento subsónico; vehículo aéreo no tripulado.

1. Introduction

The safety of the oil pipeline network is a priority requirement in the hydrocarbon industry to avoid accidents that may damage the environment and human health. Oil pipeline network requires periodic inspections to detect pipeline failures, which can cause oil leakage with long-term and irreversible impacts on both natural and human environments [1], [2]. In addition, these pipeline damages can generate oil transportation losses and high economic damages [3].

The oil leakage in a pipeline network occurs for several reasons, including material failures due to corrosion, cracks, pipe defects, incorrect operation, unreasonable design, geological hazard, and interference from third parties [4], [5], [6], [7], [8]. The geological hazard, and interference from third parties include earthquakes, floods, subsidence, implicit signage, construction works, vandalism, sabotage, overload, excavations, and illegal oil theft [9], [10], [11], [12]. Some vandalism, thefts, and sabotages on oil pipelines have been generated by people in conflict with governments or oil industries [13], [14], [15].

Furthermore, the oil pipelines could be vulnerable to terrorist attacks [15], [16]. These damage sources in the oil pipeline network can cause significant risks to the population around pipelines. These failure sources affect the safe performance of the oil pipelines. For this, inspection techniques that consider both the oil pipelines and their environment are required for monitoring defects in pipelines caused by geological hazards and interference from third parties. However, the most common processes for oil pipeline inspections (e.g., smart pigs and hydro-testing) are not suitable for pipeline damages generated by vandalism, sabotage, and illegal oil theft. For this case, other inspection techniques to detect external agents of damage to oil pipelines are required.

Researchers from UNAM have developed innovative techniques for the inspection of leaks in pipelines considering the steady-state behavior of hydraulic gradients inside pipelines [17], [18], [19]. To identify oil pipeline failures that cause oil leakage due to interference from third parties, unmanned aerial vehicles (UAVs) with infrared cameras and image processing systems can be implemented. Several researchers [20], [21], [22], [23] have designed UAVs with good results in their performances.

Pant et al. [24] implemented video stabilization algorithms for UAV-based active infrared thermography inspection. This inspection system could be applied for monitoring damage in pipelines. Kochetkova [25] reported the application of UAVs with thermal imaging cameras for monitoring large and small hydrocarbon leaks in pipelines. Nowadays, DeltaQuad Pro is a commercial UAV with a thermal vision that can be used for the inspection of oil and gas infrastructure [26].

However, this type of UAV has a high cost that limits its use. In this paper, the aerodynamic analysis of the design of a UAV with a hawk shape is reported. In this UAV, it may be adjusted a small infrared camera below its outer surface. This camera could detect the oil leakage of the pipeline network through the infrared radiation related to the oil. This UAV has a good aerodynamic behavior for its use in pipeline inspection, identifying the pipeline sections with high risks and recognizing the potential failure sources. This UAV will allow the reduction of inspection costs and inspection time in comparison with other conventional aircrafts such as helicopters or light aircraft. This UAV could be remotely controlled, keeping a stable flight. Thus, this UAV can be used for monitoring damage in pipelines that causes oil leakage in areas with difficult to access.

The aerodynamic analysis of our UAV is developed using computational fluid dynamic (CFD) models through the ANSYS-CFX software. A 1:6.5 scale

prototype of a UAV is built with a 3D printer, which is employed to obtain aerodynamic parameters (drag and lift coefficients) using experimental testing with a subsonic wind tunnel.

This paper is structured as follows: Section 2 describes the CFD modeling of the proposed UAV. Section 3 includes the results and discussion about the lift and drag coefficients of UAVs as a function of Reynolds number and angle of attack. Finally, section 4 reports the conclusions and future research.

2. CFD modeling

The proposed UAV is designed with a hawk shape (Figure 1) to take advantage of its aerodynamic configuration. The UAV wing uses the Wortmann FX 63-137 airfoil, which can allow good lift coefficients. The designed UAV has a wingspan of 2.20 m and a length of 1.49 m (Figure 2). The UAV could include a small infrared camera below its outer surface to take images of a pipeline network. These images could be processed to detect oil leakage due to interference from third parties. A GPS and a communication system of UAV will allow real-time transmission of the images (Figure 3).
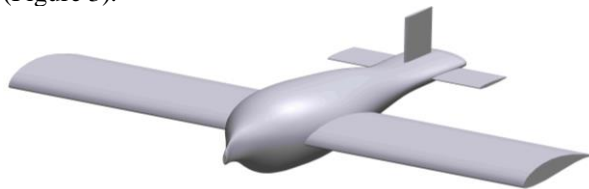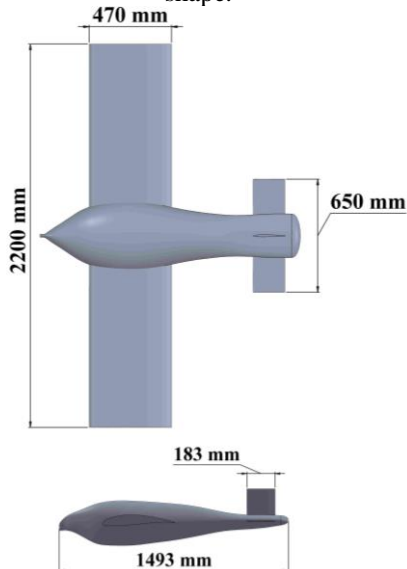

Figure 3. The schematic view of the UAV using a small infrared camera and a communication system.

The aerodynamic analysis of the UAV is obtained using a computational fluid dynamic (CFD) through the CFX module of ANSYS software. Other authors have used the ANSYS software to predict aerodynamics coefficients of UAVs with satisfactory results [27], [28]. For this aerodynamic analysis, we built a control volume to simulate the air around UAV (Figure 4). This control volume contains a cylinder that is employed to rotate the UAV. In this control, volume to simplify the numerical simulation, we were not considering the small infrared camera located below the outer surface of the UAV.

Figure 1. The design of UAV with a hawk shape.
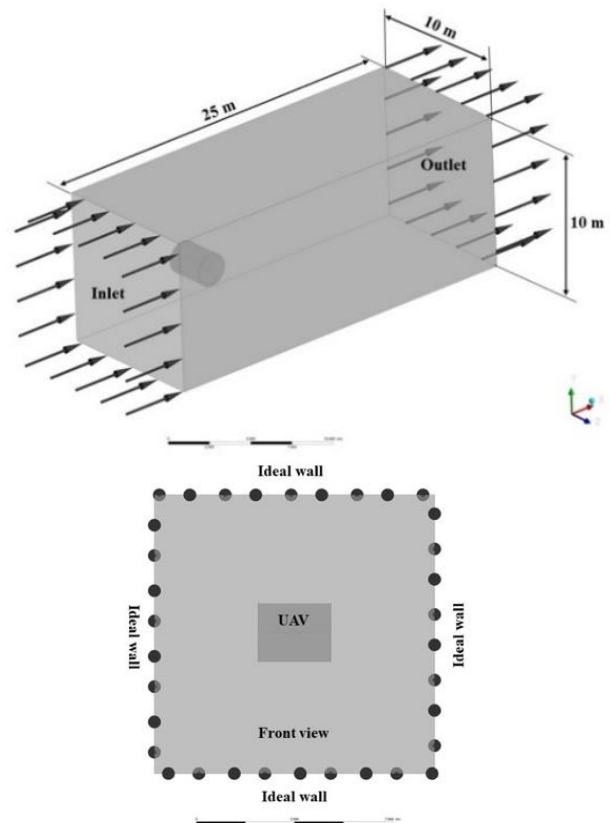

Figure 2. The dimensions of proposed UAV.

Figure 4. Control volume and boundary conditions of the UAV CFD model.

Figure 5 depicts the mesh of the control volume, that includes a fine mesh around the first layers of the outer surface of the UAV. The initial velocities along the three Cartesian components, the temperature, and air pressure are 0 m/s, 25 °C, and 1 atm, respectively. In addition, a turbulence model of Shear Stress Transport (SST) is used due to it is suitable for geometries with curvatures (e.g., aerodynamic profiles). This turbulence model considers the effects of the transition to high levels of turbulence [29].

For the convergence criterion of CFD simulation, the steady-state and a maximum residue of 1×10^{-4} were considered. In the inlet volume, a subsonic flow regime with a velocity of 20 m/s and a turbulence intensity of 5 % was regarded. In the outlet volume, a relative pressure of 0 Pa is used. The four walls of control volume and the outer surface of UAV are assumed as free slip walls (i.e., ideal walls) and as no-slip walls, respectively.
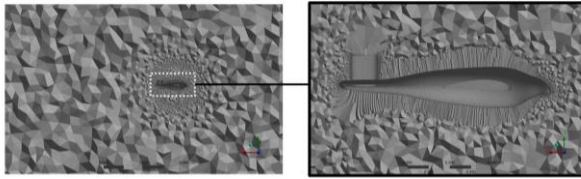

Figure 5. View of a cross-section of the mesh around the UAV CFD model.

For the aerodynamic analysis of UAVs using ANSYS software, the SST turbulence model reported in the literature [30], [31], [32], [33] was assumed. This SST model combines the best elements of $k - \varepsilon$ turbulence model and $k - \omega$ turbulence model through a blending function F_1. Both models are considered in the transition region. F_1 has value one near the wall surface and zero in the free shear flows and outer part. With these magnitudes of F_1, $k - \omega$, a model is activated in the near-wall surface. On the other hand, $k - \varepsilon$ model is employed in the rest of the flow. Thus, the SST model uses two equations of $k - \omega$ model near the wall surface and $k - \varepsilon$ model in the rest of the flow. The SST model has an upper limit for the turbulence shear stress along with boundary layers that restrict the high shear stress magnitudes. This SST model predicts the aeronautics flows with high adverse pressure gradients and separation [30]. The equations of this model for turbulent kinetic energy (k) and turbulence frequency (ω) are given by [30]:

$$\frac{\partial(\rho k)}{\partial t} + \frac{\partial(\rho U_i k)}{\partial x_i} = \tilde{P}_k - \beta^* \rho k \omega$$
$$+ \frac{\partial}{\partial x_i}\left[(\mu + \sigma_k \mu_t)\frac{\partial k}{\partial x_i}\right] \quad (1)$$

$$\frac{\partial(\rho \omega)}{\partial t} + \frac{\partial(\rho U_i \omega)}{\partial x_i} = \alpha \rho S^2$$
$$- \beta \rho \omega^2 + \frac{\partial}{\partial x_i}\left[(\mu + \sigma_\omega \mu_t)\frac{\partial \omega}{\partial x_i}\right] \quad (2)$$
$$+ 2(1 - F_1)\rho \sigma_{\omega 2} \frac{1}{\omega}\frac{\partial k}{\partial x_i}\frac{\partial \omega}{\partial x_i}$$

With

$$F_1 = tanh\left\{\left\{min\left[max\left(\frac{\sqrt{k}}{\beta^* \omega y}, \frac{500v}{y^2 \omega}\right), \frac{4\rho \sigma_{\omega 2} k}{CD_{k\omega} y^2}\right]\right\}^4\right\} \quad (3)$$

$$CD_{k\omega} = max\left(2\rho \sigma_{\omega 2}\frac{1}{\omega}\frac{\partial k}{\partial x_i}\frac{\partial \omega}{\partial x_i}, 10^{-10}\right) \quad (4)$$

where k is the turbulent kinetic energy, ρ is the fluid density, t is the time, x_i is the space coordinate component, μ is the fluid viscosity, ω is the turbulence frequency, U_i is the mean flow velocity component in the x_i-coordinate direction, S is the magnitude of the mean vorticity, v is the kinematic viscosity, y is the distance to the nearest wall surface, and $\beta, \beta^*, \alpha, \sigma_k$ and σ_ω are model constants.

The turbulent eddy viscosity (μ_t) is determined as

$$\mu_t = \frac{a_1 k}{max(a_1 \omega, SF_2)} \quad (5)$$

where a_1 is a constant and F_2 is a second blending function estimated as

$$F_2 = tanh\left[\left[max\left(\frac{2\sqrt{k}}{\beta^* \omega y}, \frac{500v}{y^2 \omega}\right)\right]^2\right] \quad (6)$$

$$\tilde{P}_k = min\left(P_k, 10\beta^* \rho k \omega\right) \quad (7)$$

$$P_k = \mu_t \frac{\partial U_i}{\partial x_j}\left(\frac{\partial U_i}{\partial x_j} + \frac{\partial U_j}{\partial x_i}\right) \quad (8)$$

The SST model coefficients β, α, σ_k and σ_ω, indicated with the symbol ϕ, are determined by blending the coefficients of the original $k - \omega$ model, considered as ϕ_1, and using those of converted $k - \varepsilon$ model, defined as ϕ_2.
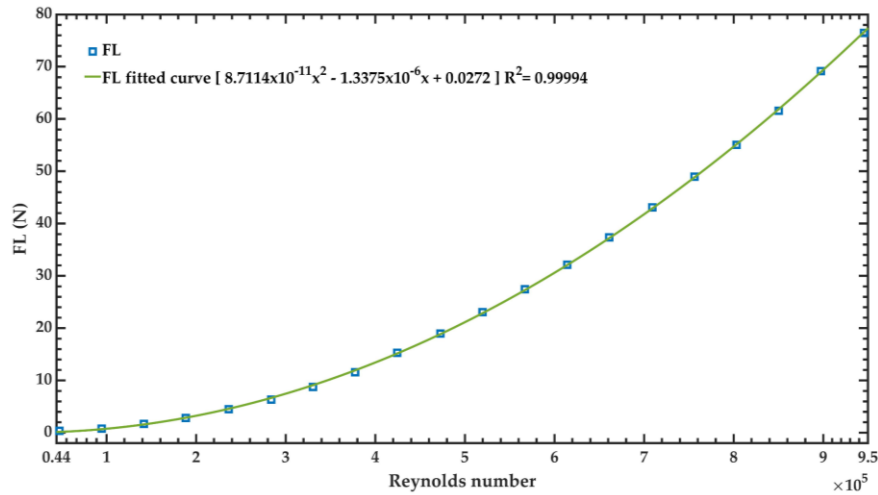
Figure 6. Lift force of UAV CFD model as a function of Reynolds number.

$$\phi = F_1\phi_1 + \left(1 - F_1\right)\phi_2 \qquad (9)$$

$$\phi = \left(\sigma_k, \sigma_\omega, \beta, \alpha\right) \qquad (10)$$

The constants for the SST model are the follows: $\beta^* = 0.09$, $\alpha_1 = 5/9$, $\beta_1 = 3/40$, $\sigma_{k1} = 0.85$, $\sigma_{\omega1} = 0.5$, $\alpha_2 = 0.44$, $\beta_2 = 0.0828$, $\sigma_{k2} = 1$, $\sigma_{\omega2} = 0.856$.

For the UAV mesh is required to know the distance between the UAV outer surface and the first layer of the mesh. This distance (Δs) can be determined by [34]:

$$\Delta s = \frac{\mu y^+}{\rho U^*} \qquad (11)$$

where y^+ is a dimensionless parameter that depends on the turbulence model, ρ is the air density and U^* is the fluid velocity when it is in contact with the geometry.

By using equation (1), a fine mesh is done around the first layers of the outer surface of the UAV. Furthermore, the characteristic length (Lc) of UAV is determined considering a rectangular section (a width and b thickness), which is given by [35]:

$$L_c = \frac{2ab}{a+b} \qquad (12)$$

The friction coefficient (C_f) of the UAV outer surface is obtained by:

$$C_f = \left[2\log(\text{Re}) - 0.65\right]^{-2.3} \qquad (13)$$

where Re is the Reynolds number.

The shear stress around the UAV outer surface is calculated by [28]:

$$\tau_w = \frac{1}{2}C_f\rho U^2 \qquad (14)$$

where U is the fluid velocity.

The fluid velocity (U^*) around the UAV outer surface is estimated as [34]:

$$U^* = \sqrt{\frac{\tau_w}{\rho}} \qquad (15)$$

The value of $y+$ is approximated as [34]:

$$y^+ = \frac{U}{U^*} \qquad (16)$$

3. Results and discussion

For the aerodynamic analysis of the UAV CFD model, we use an air velocity range between 1 and 20 m/s, keeping an angle of attack (AoA) of 0°. Figures 6 and 7 depict the lift and drag forces of the UAV CFD model as a function of its Reynolds number. The lift and drag forces increase when the Reynolds number increases. The maximum values of the lift and drag forces are 76.57 N and 7.15 N, respectively.

Figures 8 and 9 illustrate the lift and drag coefficients of the UAV CFD model as a function of Reynolds number, considering AoA of 0°. The lift coefficient increases when the Reynolds number is higher than 4×10^5.
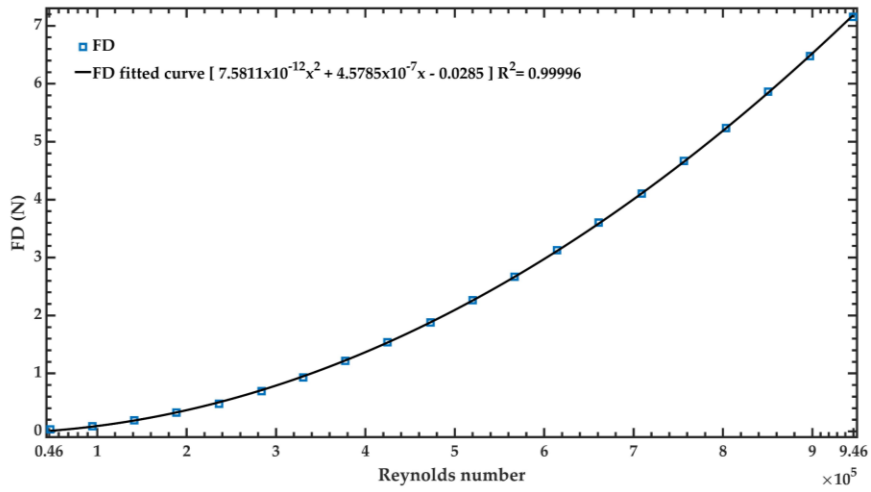
Figure 7. Drag force of the UAV CFD model as a function of Reynolds number.
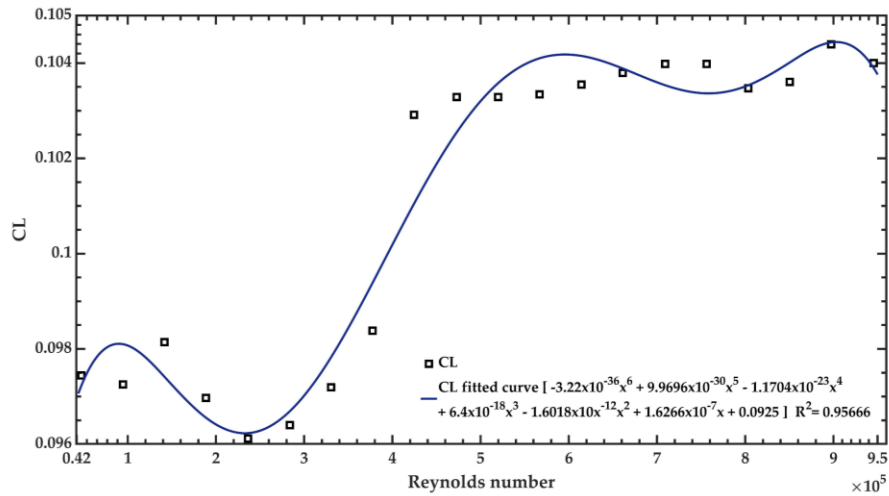

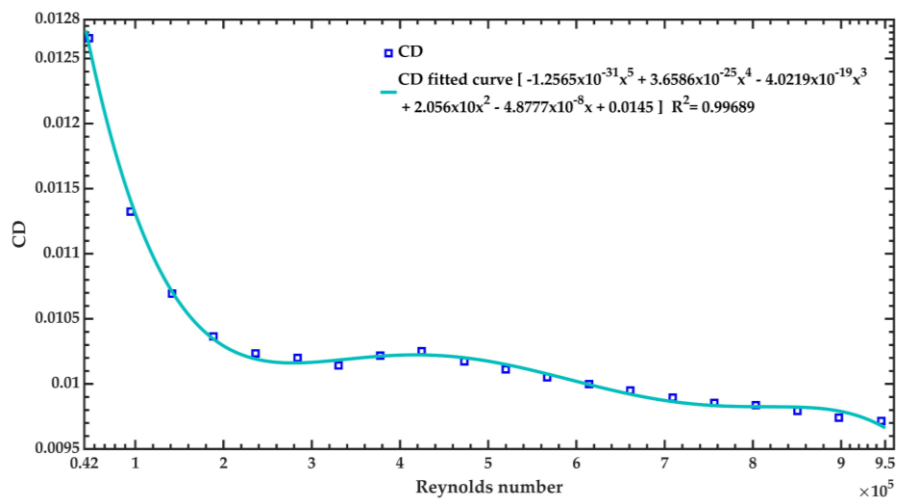Figure 8. Lift coefficient of the UAV CFD model as a function of Reynolds number.

Figure 9. Drag coefficient of the UAV CFD model as a function of Reynolds number.

On the contrary, drag force decreases when the Reynolds number is higher than 0.5×10^5. The maximum values of lift and drag coefficients are 0.1043 and 0.0126, correspondingly. In the aerodynamic analysis of the UAV CFD model, we included a range of an AoA between 0° and 22° keeping a constant velocity of 20 m/s (Figures 10 and 11).

Thus, the lift coefficient increases when AoA changes from 0 to 20°. The maximum lift coefficient (0.548) is obtained with an AoA of 20° and a velocity of 20 m/s. However, the drag coefficient decreases when the AoA is higher than 20°.

Furthermore, we determine the lift coefficient as a function of the drag coefficient for the UAV CFD model, as shown in Figure 12. In these CFD simulation results, the lift coefficient decreases when the drag coefficient overcomes the value of 0.094.

Figure 13 depicts the air velocity profile around the surface of the UAV CFD model. Figure 14 shows the air velocity profile around the wing of the UAV CFD model, in which small turbulence in the wing ends is observed. The aerodynamic coefficients of the UAV were measured using a subsonic wind tunnel of open circuit AeroLab [36].
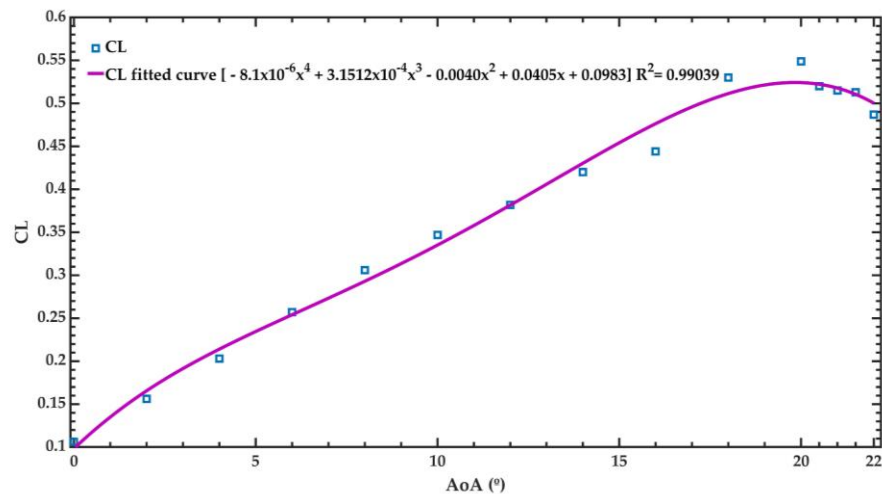

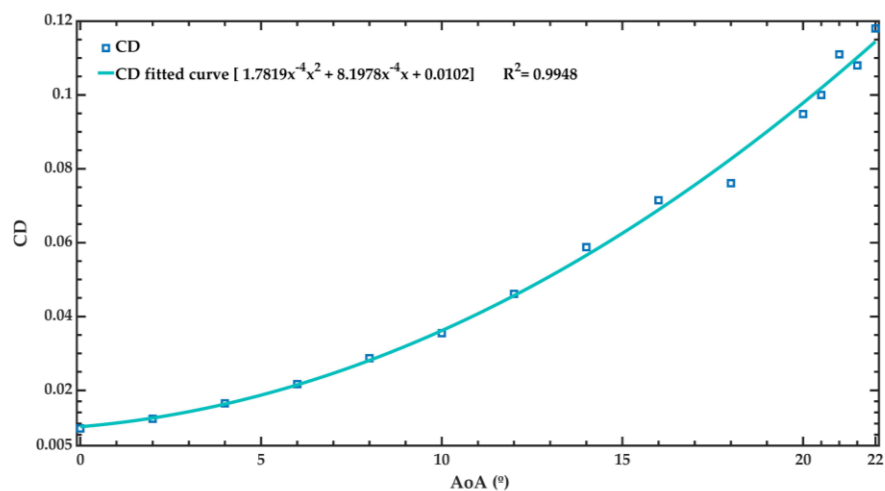Figure 10. Lift coefficient of the UAV CFD model as a function of AoA, considering the velocity of 20 m/s.

Figure 11. Drag coefficient of the UAV CFD model as a function of AoA, considering the velocity of 20 m/s.
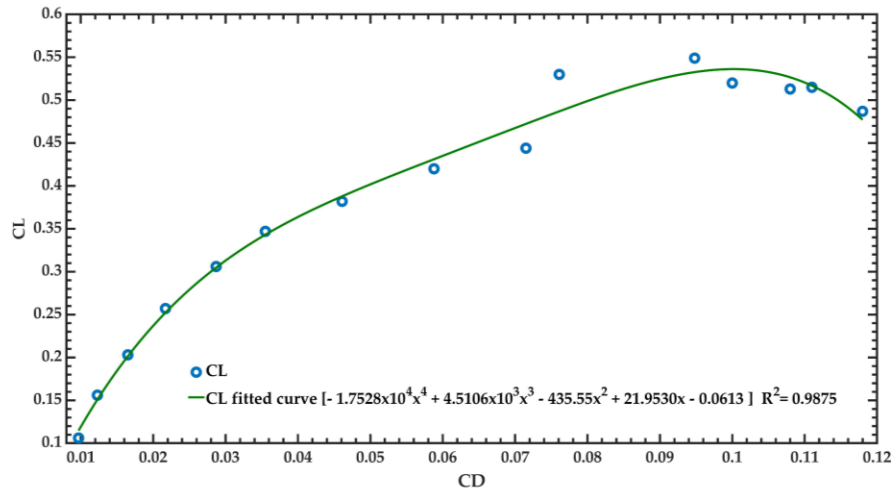
Figure 12. Lift coefficient versus drag coefficient of UAV CFD model with AoA = 22°.
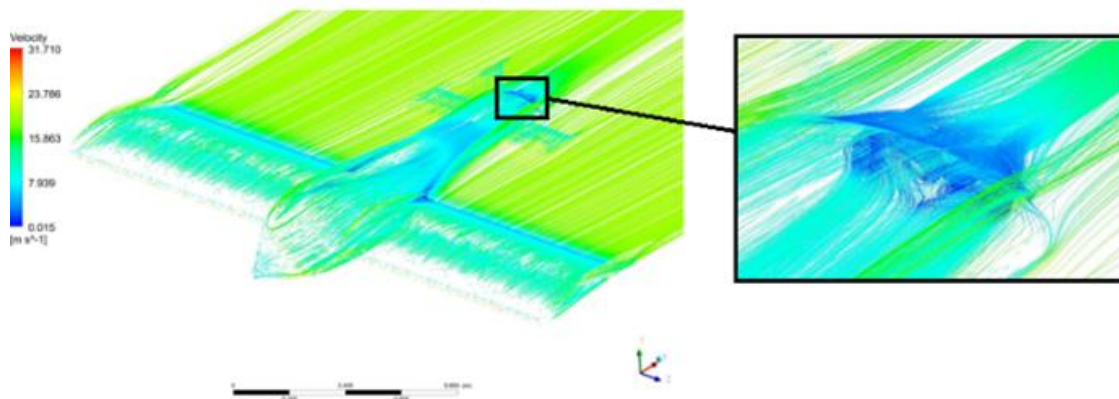

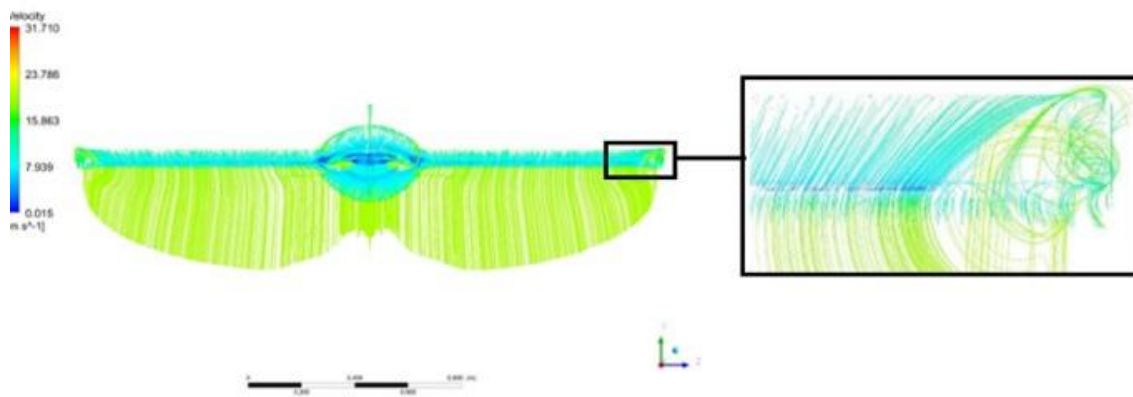Figure 13. The air velocity profile around surface of the UAV CFD model.

Figure 14. The air velocity profile around wings of the UAV CFD model.

This tunnel (Figure 15(a)) has a test section with dimensions of $0.305 \times 0.305 \times 0.610$ m. Furthermore, this tunnel has an aerodynamic balance that can measure the lift and drag forces. Also, the tunnel has a mechanism that can modify the AoA of the UAV. This mechanism is connected to a data acquisition system. For the experimental test, the UAV wing is scaled from 1.1 m to 0.25 m, and the UAV half is only used in the wind-tunnel. This UAV prototype is built through a 3D printer (Zortrax M200) and it is supported to wind tunnel through a circular bar of 3/8 inches. Thus, the UAV prototype is connected to the aerodynamic balance of the aerodynamic tunnel (Figure 15(b)).

For the experimental test, we used a similar criterion to obtain the velocities relations between the UAV prototype and the UAV CFD model. In this criterion, the UAV prototype and the UAV CFD model have equal Reynolds numbers. Table 1 shows the velocities relations between the UAV prototype and the UAV CFD model.

$$V_m = \frac{\mu_m}{\mu} \frac{\rho}{\rho_m} \frac{l}{l_m} V \qquad (17)$$

Due to the location (Mexico City) of the wind tunnel, the maximum velocity that can be obtained is 36 m/s. Thus, the maximum velocity used for the UAV prototype was 8 m/s. Figure 16 represent the experimental results of lift coefficients of the UAV prototype considering the same Reynolds numbers of the UAV CFD model. The experimental values of the lift coefficients decrease when the Reynolds number increases. The maximum and minimum values of lift coefficients are 0.126 and 0.028, respectively.

(a)   (b)

Figure 15. (a) The AeroLab subsonic wind tunnel and (b) the UAV prototype.
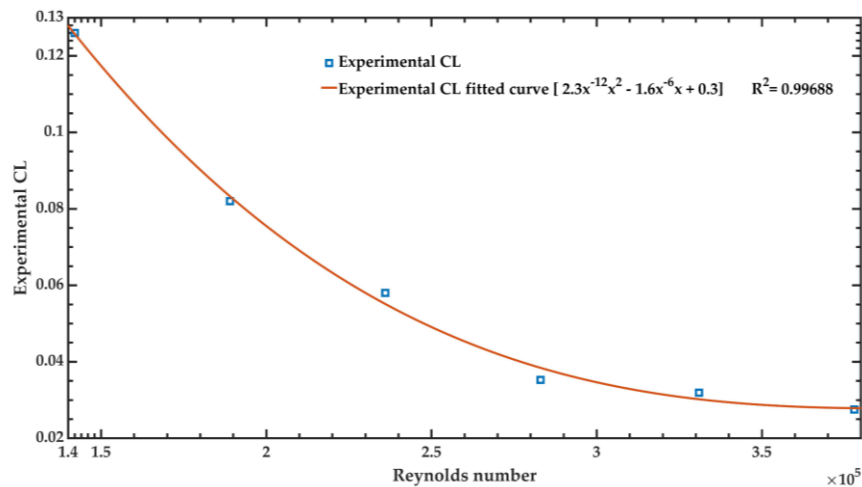

Figure 16. Experimental lift coefficient of UAV prototype using the AeroLab subsonic wind tunnel.
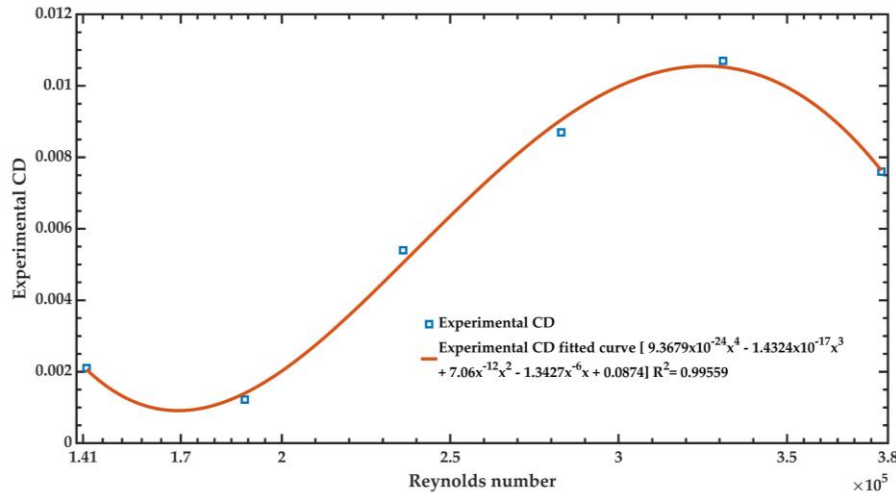
Figure 17. Experimental drag coefficient of the UAV prototype using the AeroLab subsonic wind tunnel.

Boschetti et al. [37] reported that the lift coefficient could decrease due to an increment of Reynolds numbers or the UAV geometry.

On the other hand, Figure 17 shows the experimental results of the drag coefficients of the UAV prototype. The maximum and minimum values of the drag coefficients are 0.011 and 0.001, respectively. The drag coefficients increase when the Reynolds number is higher than 1.89×10^5; however, the drag coefficient decreases when the Reynolds number overcomes 3.307×10^5. The maximum experimental values of the lift and drag coefficients are 0.126 and 0.0107, correspondingly. For the lowest value of the Reynold number, the measured lift coefficient achieved the maximum magnitude (0.126), keeping a low value of drag coefficient (0.0021). The experimental results of lift and drag coefficients of the UAV prototype are lower than those obtained from the UAV CFD model.

Table 1. Velocities relation between the UAV prototype and UAV CFD model

UAV prototype velocity (m/s)	UAV CFD model velocity (m/s)
3	13.28
4	17.71
5	22.13
6	26.56
7	30.99
8	35.42

The proposed UAV has a good aerodynamic configuration, that could allow its implementation in inspections of oil pipelines. For this, the UAV requires a small infrared camera, a GPS, and a communication system for the real-time transmission of images. The infrared camera can be collocated on the bottom surface of the UAV. This camera could identify by infrared radiation the oil leakages in pipelines caused by interference from third parties. This UAV design could detect pipeline sections with high risks and recognize the potential failure sources. The proposed UAV could decrease the inspection costs in comparison with other conventional aircrafts such as helicopters or light aircraft.

4. Conclusions

The aerodynamic analysis of a UAV (wingspan of 2.20 m and length of 1.49 m) with a hawk shape is presented. A UAV CFD model is designed to estimate their lift and drag coefficients as a function of the Reynolds number and Angles of Attack (AoA). In addition, a scaled prototype of the UAV was built through a 3D printer (Zortran 200). The left and drag coefficients were measured using a subsonic wind tunnel. For a a velocity of 20 m/s and AoA of 0°, the UAV CFD model determined lift and drag forces of 76.57 N and 7.15 N, respectively. The maximum lift coefficient (0.548) is obtained with an AoA of 20° and a velocity of 20 m/s. A small infrared camera, a GPS, and a communication system could be implemented on the bottom surface of the proposed UAV. Thus, the UAV could detect oil leakage in the pipeline network caused by interference from third parties, including sabotage, vandalism, excavations, and illegal oil theft.

For future research work, we will build the UAV with its infrared camera and control system.

Acknowledgment

References

[1] T. Shu-Jiao, W. Zong-Zhi, W. Ru-Jun, W. Hao, "Fire risk study of long-distance oil and gas pipeline based on QRA," *Procedia Eng*., vol. 135, pp. 369-375, 2016, doi: 10.1016/j.proeng.2016.01.144

[2] C. Gómez, D.R. Green, "Small unmanned airborne systems to support oil and gas pipeline monitoring and mapping," *Arab. J. Geosci*., vol. 10, no. 202, pp. 1-17, 2017. doi: 10.1007/s12517-017-2989-x

[3] D. Rifai, A.N. Abdalla, R. Razali, K. Ali, M.A. Faraj, "An Eddy current testing platform system for pipe defect inspection based on an optimized Eddy current technique probe design," *Sensors*, vol. 17, no. 3, pp. 579, 2017. doi: 10.3390/s17030579

[4] H. Iqbal, S. Tesfamariam, H. Haider, R. Sadiq, "Inspection and maintenance of oil & gas pipelines: a review of policies," *Struct. Infrastruct. Eng*., vol. 13, no. 6, pp. 794-815, 2016. doi: 10.1080/15732479.2016.1187632

[5] Mohamed, M.S. Hamdi, S. Tahar, "Using Computational Intelligence for the Safety Assessment of Oil and Gas Pipelines: A Survey," in *Data Science and Big Data: An Environment of Computational Intelligence. Studies in Big Data*, Pedrycz, W., Chen, S.M., Eds.; Cham: Springer International Publishing, 2017, pp. 189-207.

[6] Y. Guo, X. Meng, D. Wang, T. Meng, S. Liu, "Comprehensive risk evaluation of long-distance oil and gas transportation pipelines using a fuzzy Petri net model," *J. Nat. Gas Sci. Eng*., vol. 33, pp. 18-29, 2016. doi: 10.1016/j.jngse.2016.04.052

[7] S. B. Da Cunha, "A review of quantitative risk assessment of onshore pipelines," *J. Loss Prev. Proc. Ind.*, vol. 44, pp. 282-298, 2016. doi: 10.1016/j.jlp.2016.09.016

[8] Q. Zhou, W. Wu, D. Liu, K. Li, Q. Qiao, "Estimation of corrosion failure likelihood of oil and gas pipeline based on fuzzy logic approach," *Eng. Fail. Anal*., vol. 70 pp. 48-55, 2016. doi: 10.1016/j.engfailanal.2016.07.014

[9] D. Yuhua, Y. Datao, "Estimation of failure probability of oil and gas transmission pipelines by fuzzy fault tree analysis," *J. Loss Prev. Proc. Ind*., vol. 18, no. 2, pp. 83-88, 2005. doi: 10.1016/j.jlp.2004.12.003

[10] W. Liang, J. Hu, L. Zhang, C. Guo, W. Lin, "Assessing and classifying risk of pipeline third-party interference based on fault tree and SOM," *Eng. Appl. Artif. Intel.*, vol. 25, no. 3, pp. 594-608, 2012. doi: 10.1016/j.engappai.2011.08.010

[11] C. O. Okpo, R. C. Eze, "Vandalization of oil pipelines in the niger Delta region of Nigeria and poverty: an overview," *Stud. Sociol. Sci*., vol. 3, no. 2, pp. 13-21, 2012. doi: 10.3968/j.sss.1923018420120302.2950

[12] R. Standard, 2014. Police probe theft of oil from pipeline under Nick Clegg's country residence - Crime, London Evening Standard [Online]. Available: http://www.standard.co.uk/news/crime/police-probe-theft-of-oil-from-pipeline-under-nickcleggs-country-residence-9659184.html

[13] P. E. Igbinovia, *Oil Thefts and Pipeline Vandalization in Nigeria*. Ibadan, Nigeria: Safari Books, 2014.

[14] J. Sun, Z. Zhang, X. Sun, "The intelligent crude oil anti-theft system Based on IoT under different scenarios," *Proc. Comp. Sci*., vol. 96, pp. 1581-1588, 2016. doi: 10.1016/j.procs.2016.08.205

[15] P. W. Parfomak, Keeping America's pipelines safe and secure: key issues for congress, Congressional Research Service, 2011 [Online]. Available: http://fas.org/sgp/crs/homesec/R41536.pdf

[16] J. Eze, C. Nwagboso, P. Georgakis, "Framework for integrated oil pipeline monitoring and incident mitigation systems," *Rob. Comp. Integ. Manuf*., vol. 47, pp. 44-52, 2017. doi: 10.1016/j.rcim.2016.12.007

[17] L. Torres, C. Verde, L. Molina, "Leak diagnosis for pipelines with multiple branches based on model similarity," *J. Process Control,* vol. 99, pp. 41-53, 2021. doi: 10.1016/j.jprocont.2020.12.003

[18] C. Verde, L. Torres, O. González, "Descentralized scheme for leaks' location in a branched pipeline," *J. Loss Prev. Process Ind.,* vol. 43, pp. 18-28, 2016. doi: 10.1016/j.jlp.2016.03.023

[19] O. González, C. Verde, L. Torres, "Leak estimation method for complex pipelines with branch juctions," *J. Press. Vessel Technol.,* vol. 139, no. 2, pp. 021701, 2017. doi: 10.1115/1.4034403

[20] Sóbester, A.J. Keane, J. Scanlan, N.W. "Bressloff, Conceptual design of UAV airframes using a generic geometry service," In *Proceedings of the Infotech@Aerospace Conferences, Arlington,* VA, USA, 2005, pp. 26-29. doi: 10.2514/6.2005-7079

[21] L. Jung-Ryul, C. Chang Min, P. Chan Yik, T Chung Thanh, S. Hye Jin, J. Hyomi, B. F. Eric, "Spar disbond visualization in in-service composite UAV with ultrasonic propagation imager," *Aerosp. Sci. Technol.* vol. 45, pp. 180-185, 2015. doi: 10.1016/j.ast.2015.05.010

[22] P. Panagiotou, P. Kaparos, C. Salpingidou, K. Yakinthos, "Aerodynamic design of a MALE UAV," *Aerosp. Sci. Technol.*, vol. 50, pp. 127-138, 2016. doi: 10.1016/j.ast.2015.12.033

[23] P. Panagiotou, S. Fotiadis-Karras, K. Yakinthos, "Conceptual design of a Blended Wing Body MALE UAV," *Aerosp. Sci. Technol.,* vol. 73, pp. 32-47, 2018. doi: 10.1016/j.ast.2017.11.032

[24] S. Pant, P. Nooralishahi, N.P. Avdelidis, C. Ibarra-Castanedo, M. Genest, S. Deane, J.J. Valdes, A. Zolotas, X. P. V. Maldague, "Evaluation and Selection of Video Stabilization Techniques for UAV-Based Active Infrared Thermography Application," *Sensors,* vol. 21, no. 5, pp. 1604, 2021. doi: 10.3390/s21051604

[25] L.I. Kochetkova, "Pipeline monitoring with unmanned aerial vehicles," *J. Phys. Conf. Ser.*, vol. 1015, no. 4, pp. 20-21, 2021. doi: 10.1088/1742-6596/1015/4/042021

[26] Vertical Technologies, " DeltaQuad PRO # VIEW," 2021 [Online]. Available: https://www.deltaquad.com/vtol-drones/view/#specifications

[27] B. Raeisi, H. Alighanbari, "Effects of tilting rate variations on the aerodynamics of the tilting ducted fans mounted at the wing tips of a vertical take-off and landing unmanned aerial vehicle," *Proc. IMechE Part G: J. Aerosp. Eng.*, vol. 232, no. 10, pp. 1803-1813, 2018. doi: 10.1177/0954410017703146

[28] X. Du, A. Dori, E. Divo, V. Huayamave, F. Zhu, "Modeling the motion of small unmanned aerial system (sUAS) due to ground collision," *Proc. IMechE Part G: J Aerosp. Eng.*, vol. 232, no. 10, pp. 1961-1970, 2018. doi: 10.1177/0954410017705903

[29] P. D. Bravo-Mosquera, L. Botero-Bolivar, D. Acevedo-Giraldo, H. D. Cerón-Muñoz, "Aerodynamic design analysis of a UAV for superficial research of volcanic environments," *Aerosp. Sci. Technol.*, vol. 70, pp. 600-614, 2017. doi: 10.1016/j.ast.2017.09.005

[30] F. R. Menter, M. Kuntz, R. Langtry, "Ten years of industrial experience with the SST turbulence model," in *Turbulence, Heat and Mass Transfer 4,* K. Hanjalic, Y. Nagano, M. Tummers (Eds.), New York, NY: Begell House Inc, 2003, pp. 625-632.

[31] F. R. Menter, Zonal two equation k–ω turbulence models for aerodynamic flows. Sunnyvale, CA, USA: AIAA, 1993.

[32] F. Menter, C.J. Ferreira, T. Esch, B. Konno, "The SST Turbulence Model with Improved Wall Treatment for Heat Transfer Predictions in Gas Turbines," in *International Gas Turbine Congress 2003, Tokyo, IGTC2003-TS-059*, 2003, pp. 2-7.

[33] J. E. Bardina, P. G. Huang, T. J. Coakley, "Turbulence Modeling, Validation, Testing and Development," in *NASA Technical Memorandum 110446*, 1997.

[34] H. Schlichting, K. Gersten, *Boundary-Layer Theory*. 9th ed., Berlin: Springer Nature, 2017.

[35] Y. Cengel, *Fluid Mechanics Fundamentals and Applications*. 3rd ed. New York, NY, USA: McGraw-Hill Education, 2013.

[36] AeroLab, "Educational Wind Tunnel Operations Manual," University of Colorado Boulder, 2012.

[37] P. J. Boschetti, E. M. Cárdenas, A. Amerio, *Aerodynamic optimization of an UAV design*. Arlington, VA, USA: American Institute of Aeronautics and Astronautics, 2005. doi: 10.2514/6.2005-7399